IDENTIFICATION OF COUPLED NATURAL FREQUENCIES IN A ROTOR-STATOR TEST-RIG FOR DIFFERENT GAS PROPERTIES

B. Barabas, D. Brillert, H. J. Dohmen, F.-K. Benra

University of Duisburg-Essen, Chair of Turbomachinery, Duisburg, Germany
botond.barabas@uni-due.de

ABSTRACT

In this paper a rotor-stator cavity test rig for experimental investigations of acoustic fluid-structure interactions in side cavities of radial compressors is introduced. The instrumentation of the test rig and the evaluation methodology are presented. The fluid is excited at frequencies, which are independent from the disk rotational speed, with loudspeakers. The acoustic pressure patterns are detected with a pressure sensor rotatable in circumferential direction.

The gas properties are varied via different pressure levels in the test rig. First experimental results of natural frequencies are presented. The structure and acoustic dominant m = 4, n = 0, l = 1 modes have been excited and identified. The experimental results of the resonance frequencies of coupled modes on the dependence of the surrounding gas pressure are compared to a coupled numerical modal analysis and an analytical approach of other researchers. The main trend is in good accordance to them.

ACOUSTICS, ROTOR-STATOR CAVITY, NATURAL FREQUENCY

NOMENCLATURE

Latin symbols		
b, s	[m]	Thickness of disk, axial gap width
c	[m/s]	Speed of sound
*f, f**	[1/s], [-]	Frequency, dimensionless frequency related to the acoustic dominant natural frequency (m_{ac} = 4, n_{ac} = 0, l_{ac} = 1)
l	[-]	Axial order (number of axial nodes)
m	[-]	Circumferential order (number of diametral nodes)
n	[-]	Radial order (number of node circles)
p	[bar]	Pressure
$S_{max,exc}$	[Hz/s]	Maximum sweep velocity
Greek symbols		
α	[°]	Angle in circumferential direction
ρ	[kg/m^3]	Density
Δω, ω	[1/s]	Frequency difference in radian, frequency in radian
ζ*	[-]	Dimensionless critical damping ratio related to the critical damping ratio of the structure dominant eigenmode (m_{sc} = 4, n_{st} = 0)
Indices		
ac		Acoustic
f		Fluid
r		Resonance
st		Structure

INTRODUCTION

The application of high pressure radial compressors is expected to have an above-average growth rate in future. The main application fields of these machines are assumed at oil exploitation sites as re-injection gas supplies or at Carbon-Capture-and-Storage power plants for carbon dioxide compression. Thus, operational pressures and densities of the working fluids are intended to increase, which raises the influence of aeroacoustics and aeroelasticity in side cavities of radial compressors on their operational reliability.

A fundamental aeroacoustic excitation source in turbomachines has been published by Tyler and Sofrin (1961). They reveal excitations at discrete frequencies as an interaction between rotor and stator components, the so called Tyler-Sofrin modes. Further studies have been conducted by Ehrich (1969), who focuses on natural frequencies of acoustic modes in annular cavities influenced by axial flow and flow rotation. A problem orientated numerical investigation of acoustic modes in the side cavities of radial compressors has been conducted by König (2009), who reveals a coupling of the acoustic modes in the two side cavities with each other. The paper compares 2D-analytical and 3D-FEM methods for acoustic mode calculations. Petry (2011) has first shown experimentally the excitation of acoustic resonances in side cavities of radial compressors by Tyler-Sofrin modes.

When vibrations are matter of investigations, impellers surrounded by dense gases cannot be treated separately but as a coupled system comprising the impeller structure and the fluid. Each nodal diameter natural mode is at least split into two modes with two corresponding natural frequencies. For a weak coupling the coupled natural frequencies approximately equal the uncoupled structural and acoustic natural frequency, respectively.

The effect of dense surrounding fluids on the natural frequencies of pump impellers has been investigated numerically by Liang et al. (2007) and experimentally by Rodriguez et al. (2006). Their findings are decreasing natural frequencies of the impeller and increasing damping ratios if the impeller is surrounded by water instead of air. Magara et al. (2013) have investigated the natural frequencies of a radial compressor impeller for different surrounding gas pressures experimentally. Their results show for some natural frequencies of the structure a decreasing trend for increased pressures, however, other natural frequencies increase at the same time. They conclude an influence of the stiffness of the surrounding gas beside the added mass effect onto the structure.

Sandberg and Göransson (1988) have conducted a numerical finite element approach to investigate a coupled fluid-structure interaction of an aircraft fuselage. They have found striking differences between the uncoupled and coupled eigenfrequencies. In their numerical investigation of coupled eigenmodes of a nuclear vessel Sigrist et al. (2006) discover a change of mode shapes at increasing fluid densities. This effect is observed in the results when added mass and coupling effects are taken numerically into account.

It becomes apparent that aeroelasticity and aeroacoustics in side cavities of radial compressors is a complex research field. Investigations in the past have revealed some effects, which cannot be fully described, yet. In order to gather fundamental understanding of the effects a rotor-stator test rig has been built up at the University of Duisburg-Essen. The main advantage of its design is that contrary to real compressors the excitation frequency and strength can be set independently from gas parameters and disk rotational speeds. This decoupling of excitation source and the system, which should be excited, allows the identification of influence parameters. The results, which are presented within this paper, show the influence of an increased pressure on coupled modes. The experimental data are gathered with a non-rotating disk.

TEST RIG

The acoustic measurements are conducted in the rotor-stator test rig that has been introduced in the framework of aerodynamic measurements in Barabas et al. (2015). Compared to the aerodynamic version the main parameters remain unchanged. However, some acoustic specific instrumentation has been installed additionally.

The test rig represents geometrically simplified side cavities of radial compressors. In Figure 1 a radial compressor stage is sketched. The side cavities are the spaces between the casing and the impeller's hub and shroud. They are marked green and blue in Figure 1, respectively. These cavities are simplified in the test rig (Figure 2). The impeller represented as a plain aluminum disk is embraced by a plain walled casing. The test rig's cavities are called rear and front cavity. The sensors' and loudspeaker's allocations are sketched in the figure, too. The axial gap widths (*s*) in both cavities can be adjusted independently from each other covering the range of gap widths of modern radial compressors. Within this experimental investigation the gap widths in both cavities are set equally. The disk thickness (*b*) has been chosen to enforce at least one pair of acoustic and structural modes, with the same number of nodal diameters, to have similar natural frequencies at ambient conditions. Thus, this ensures a strong coupling between the acoustic and structural mode.

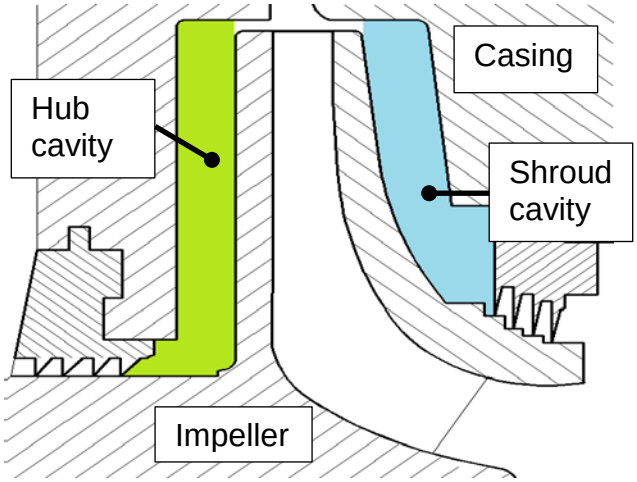

Figure 1: A meridional sketch of a radial compressor stage with the side cavities.

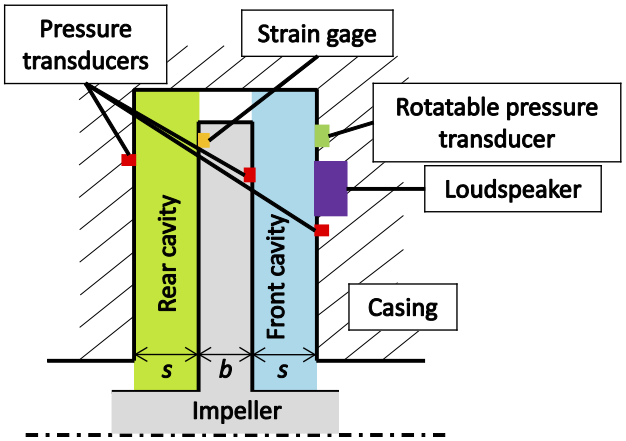

Figure 2: Sketch of the rotor-stator test rig with the acoustic specific instrumentation (meridional view).

A picture of the test rig, taken from the front cavity side, is presented in Figure 3. In Figure 4 the test rig is sketched in the normal view with the sensor positions. The pressure sensors are marked with a "P", the strain gages with a "G", and "LS" refers to the loudspeakers. The character inside the parentheses represents the location: The rear cavity is labeled with "RC" and the disk is labeled with "D". If the location character is omitted the sensor is mounted in the front cavity. The presented results within this paper have been recorded with the pressure sensor "P147" and the strain gage "G141 (D)", mounted on the disk. The fluid is excited with the loudspeaker "LS 2". For a better differentiation they are marked red in the figure.

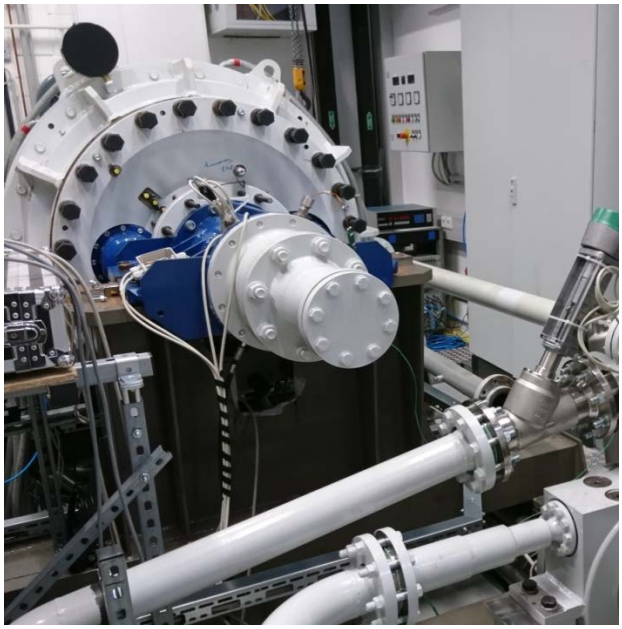

Figure 3: A picture of the test rig.

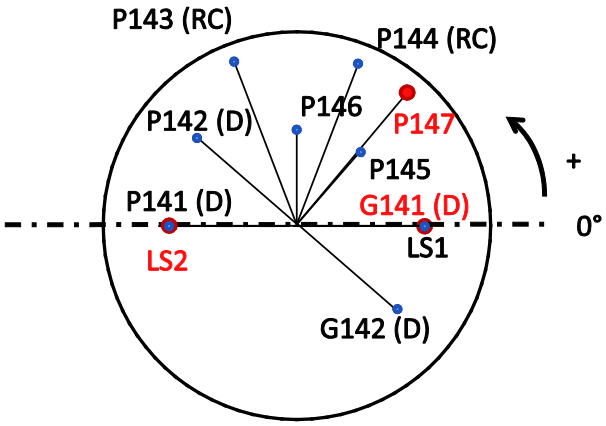

Figure 4: Normal view of the rotor-stator test rig with the sensors' allocation. Within this paper results of the red marked sensors are presented. Labels: "P": pressure sensor, "G": strain gage, "LS": loudspeaker, "RC": rear cavity, "D": disk

In Figure 5 and Figure 6 results of a numerical modal analysis with the selected mode shape of the structure and acoustic dominant mode are displayed. The disk is illustrated from the front cavity side with the acoustic pressure pattern on its surface. For a better view the fluid volume is removed from the figure. The mode has four nodal diameters (m = 4) and zero nodal circles (n = 0). The pressure pattern on the rear side of the disk is reversed, that means one axial node (l = 1) for the acoustic mode exists in the radial gap over the disk. This axial node is important to cause a resulting force onto the disk.

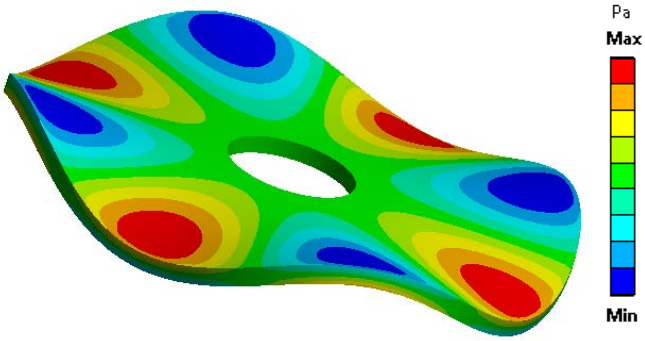

Figure 5: Structure dominant (in-phase) mode with four nodal diameters and zero nodal circles. The disk is displayed with the acoustic pressure pattern. Result of the numerical modal analysis.

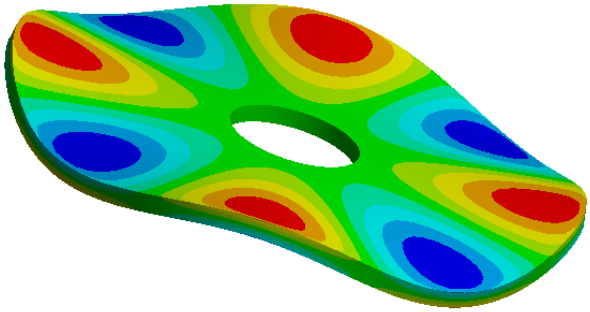

Figure 6: Acoustic dominant (out-of-phase) mode with four nodal diameters and zero nodal circles. The disk is displayed with the acoustic pressure pattern. Result of the numerical modal analysis.

The disk is mounted on a shaft, which is coupled via a magnetic coupling to the continuously adjustable high-speed electrical drive. The magnetic coupling allows a torque transmission into the sealed zero-leakage casing, which can be pressurized with various gas compositions. A separate pre-mix chamber upstream the test rig lets maintaining equal gas mixtures at different pressure levels. The gas fractions are set with their respective partial pressures.

Instrumentation

The results of the experiments should give a better understanding about the behavior of acoustic modes, their modal damping, and the fluid structure interaction. Hence, pressure sensors are needed

to characterize the acoustic pressure perturbation and strain gages are essential to sense structural strain to conclude the vibration of the disk.

Moreover, the test rig has some specific instrumentation, on the one hand due to design constraints and on the other hand to simplify the identification of acoustic modes. The impeller is a bladeless disk, thus, the blade-vane interaction as the main excitation source is missing. Two loudspeakers mounted in the casing of the front cavity serve as the substitute for the missing rotor-stator excitation. The loudspeakers are installed in circumferential direction directly opposite to each other. The excitation frequency is set by an Agilent 33120A wave generator and amplified with an amplifier. The output power of the loudspeakers is high enough to excite acoustic modes in the test rig's cavities, thus, serving as a substitute for the missing rotor-stator interaction. The loudspeakers can be driven in double or single mode of operation, depending on whether even or odd radial modes should be excited.

The applied acoustic specific transducers are summarized in Table 1. The transducer positions in meridional view and in normal view are presented in Figure 2 and Figure 4, respectively.

The positions and orientations of the two strain gages, mounted on the rear side of the disk, have been pre-estimated with a numerical modal analysis of the disk. The calculation reveals the highest strain for low mode order investigations if they were mounted radially far outwards and orientated in tangential direction. The angle between both transducers allows a determination of low order modes with respect to their phase.

A numerical modal analysis of the cavity has been conducted, too, to define the best locations of the pressure sensors. The results show high pressure gradients, when low order acoustic modes are excited, radially far outside. Contrary, two pressure sensors are mounted on an inner radial position to allow the identification of acoustic modes with a nodal circle. Similar to the strain gages, the chosen angles between the transducers allow a determination of low order modes with respect to their phase. However, even the identification of low order modes is an impossible task with a finite number of pressure transducers. As remedy, a novel rotatable pressure transducer has been developed and built in the front cavity casing of the test rig. It is based on an idea of rotatable microphones (Cicon, 1982). Together with a specific evaluation method the pressure pattern of an acoustic mode at a constant excitation frequency can be obtained in circumferential direction.

Place of installation	**Type of transducer**	**Quantity**
Impeller	Strain gage	2
Impeller	Piezoresistive pressure transducer	2
Rear cavity	Piezoresistive pressure transducer	2
Front cavity	Piezoelectric pressure transducer	2
Front cavity (Rotatable transducer)	Piezoelectric pressure transducer	1

Table 1: Summary of the measurement instrumentation.

THEORETICAL APPROACH

The experimental results are compared with a numerical modal analysis and a qualitative analytical approach presented by Magara et al. (2008).

The numerical modal analysis is conducted with Ansys Mechanical as a coupled fluid-structure modal analysis. The geometry of the cavity and the disk is simplified, the loudspeakers' holes and the shaft are neglected. The parts are meshed with hexahedron elements and a mesh independence of the results has been established. Calculations have been performed with fluid properties set to the experimental ones as listed in Table 2.

Magara et al. (2008) propose a qualitative analytical approach to estimate the natural frequency shift of a similar coupled system with a disk enclosed in a gas cavity. They couple the equations of motions of the gas and the structure and assume an inviscid and compressible gas. They obtain

$$\left(\omega_{\mathrm{ac,r}}^2-\omega^2\right)\left(\omega_{\mathrm{st,r}}^2-\omega^2\right)-2\omega^2\frac{\rho_{\mathrm{f}}\cdot c^2}{\rho_{\mathrm{st}}\cdot bs}=0 \quad (1)$$

with $\omega_{\mathrm{ac,r}}$ and $\omega_{\mathrm{st,r}}$ as the uncoupled natural frequencies of the fluid and disk, respectively. ρ_{f} and ρ_{st} correspond to the density of the fluid and the structure. The fluid's speed of sound is denoted with *c* and the geometry is represented by *b* as the disk thickness and *s* as the axial gap width of the cavity (Figure 2). The minuend of Equation (1) can be graphically represented as a parabola, the subtrahend as a line. Two solutions exist at the cross-sections. These are the coupled natural frequencies of the system. Magara et al. (2008) have introduced the terms "disc origin" and "fluid origin mode" for the respective branches of the parabola, depending on the uncoupled natural frequencies. The terms are renamed to "structure dominant" and "acoustic dominant" within this paper. The vibration can be characterized with the phase relation between the axial disk motion and the pressure pattern's resulting axial force onto the disk, too. In the model of Magara the lower frequency branch is called "in-phase mode" (Figure 5) and the higher frequency branch "out-of-phase mode" (Figure 6).

The uncoupled natural frequencies $\omega_{\mathrm{ac,r}}$ and $\omega_{\mathrm{st,r}}$ for Equation (1) have been determined via solving it with the experimental data from the 1 bar case.

METHODOLOGY

Experimental Procedure and Boundary Conditions

The basis for the evaluation of the natural frequencies and the modal damping values are frequency sweep experiments over a specific interval. The maximum allowed sweep velocity $S_{\mathrm{max,exc}}$ without falsifying the measured resonance height, frequency, and damping is set according to Ewins (1995) to

$$S_{\mathrm{max,exc}}=3.6\cdot f_r^2\zeta^2 \quad (2)$$

with f_r as the resonance frequency and ζ as the critical damping ratio. The procedure for a sweep experiment is presented exemplary:

1. The fluid properties are set in the test rig and a good mixture inside the cavities is ensured. All experiments referred to in this paper have been conducted with air at different pressure levels. The boundary conditions of all experiments are summarized in Table 2.
2. All measurements in this publication have been conducted with a stationary disk. To get comparable results from the sensors mounted on the disk it is turned to a reference position.
3. The frequency sweep with a constant sweep velocity is executed and the data is recorded.

Pressure level [bar]	Density [kg/m^3]	Speed of sound [m/s]
1	1.19	343.6
1.5	1.89	343.0
2	2.39	343.1
2.5	2.97	343.2
4	4.77	343.4
7	8.29	344.1

Table 2: Summary of the experimental boundary conditions.

The identification of the modes excited during the experiments is very important for the classification of the results. Therefore, the mentioned coupled FEM modal analysis and an experimental modal hammer test of the disk have been conducted prior the measurements.

Modes of vibration in reality can differ from ideal results, due to material and geometrical imperfections. Hence, the developed pressure patterns at specific frequencies have to be measured

during the experiments. The rotatable pressure transducer is used for this. Its measuring range in circumferential direction is 300°. The experimental procedure to record the data for the pressure pattern is presented exemplary:

1. The fluid properties are set in the test rig and a good mixture inside the cavities is ensured.
2. A constant excitation frequency is set.
3. The rotatable pressure transducer is rotated to a specific circumferential position.
4. Pressure data at that position is acquired.
5. Steps 3. and 4. are repeated for all circumferential positions with a constant angle difference in between.

Together with a specific evaluation procedure quasi snap-shots of the pressure fluctuations in circumferential direction can be generated.

Uncertainty and Repeatability Analysis

The results presented in this paper are based on a test campaign in which not all sweep experiments have been repeated. Thus, the results cannot be interpreted statistically. However, to show the repeatability of the experiments evaluated results of different sweep runs (blue and red markers) are presented in Figure 7. Additionally, in Table 3 the ratios between the different sweep runs are shown. Regarding the resonance frequency the deviation is less than 1 %. The amplitude ratio has a maximum relative difference of 5 %. Finally, the variation of the damping ratio, which has been determined with the half-power point method as described in Ewins (1995), is up to 8 %. For the resonance frequency a good accordance between different measurements is achieved. The damping, on which it is not focused in this paper, shows larger deviations. In future experimental campaigns, when the damping is a matter of investigation, the number of sweep runs with equal boundary conditions has to be increased to minimize the statistical error.

The uncertainty of the measurement equipment is not considered in this framework, because results are interpreted regarding their relative differences, for which the absolute uncertainties do not play a role.

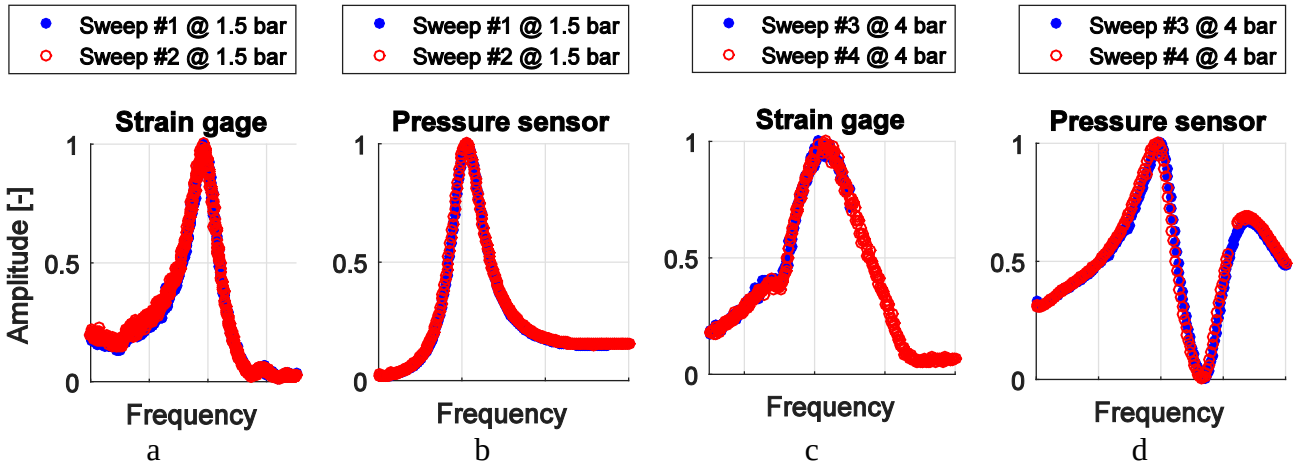

Figure 7: Comparison of repeated measurements at different boundary conditions and recorded with different sensors. The evaluated STFT results are compared.

	Sweep #1/#2			Sweep #3/#4		
	Resonance frequency ratio	Damping ratio	Amplitude ratio	Resonance frequency ratio	Damping ratio	Amplitude ratio
Strain gage	1.0005	0.92	0.98	0.9989	1.03	1.00
Pressure sensor	1.0001	0.98	0.95	1.0002	0.97	1.00

Table 3: Modal properties' ratios of different sweep runs and for different sensors.

Evaluation Procedure

The evaluation of the measured data during a sweep experiment is performed with a Short Time Fourier Transformation (STFT) in Matlab®. The blocks have been chosen small enough to allow a good resolution in time and with an overlap of 75% to avoid data loss. With the knowledge and application of the excitation frequency to time relation, a good frequency resolution can be achieved, too.

However, there is a crucial issue regarding the analysis of the response data measured with the pressure transducers and strain gages: The excitation force cannot be determined directly. The loudspeaker power in dependence of fluid parameters could not be revealed during this experimental campaign. Hence, the Frequency Response Function (FRF) is not calculated. The analysis is based on the direct response of the transducers, not set in relation to the excitation force. Comparisons of the response signals between different pressure levels should be treated with caution, though, within one pressure level the excitation force should remain equal allowing a comparison.

The evaluation procedure of the rotatable pressure sensor is based on the loudspeaker excitation signal as the reference. The harmonic reference signal crosses its mean value once in a certain direction in each period. During the evaluation process this crossing is detected and the pressure of the rotatable sensor is determined at a constant time difference in relation to that crossing. The variation of the time difference's length yields a pressure signal at different phases. At each circumferential position the mean pressure value of 500 periods is determined. They are plotted over the geometrical circumferential angle of the cavity. This procedure is repeated for different time differences between the reference signal's crossings and the rotatable pressure sensor's signal.

RESULTS

Identification of Modes

Experimental results in the frequency domain of the strain gage mounted at the disk and the pressure sensor P147 in the front cavity fixed at 50° circumferential position are presented with a variation of the pressure level inside the test rig in the waterfall plots in Figure 8 and Figure 9. The response amplitudes are divided by the maximum amplitude of the respective sensor. They are plotted over a frequency f^* based on the acoustic dominant natural frequency of the $m_{ac} = 4$, $n_{ac} = 0$, $l_{ac} = 1$ mode at 1 bar. The variation of the pressure level corresponds with the third axis pointing to the rear. The gaps between $f^* = 0.94 \ldots 0.96$ for the pressure levels from 1.5 to 4 bar arise from lacking experimental data. The strain gage results at 1 bar show two peaks: A relatively flat one at $f^* = 1$ and a relatively sharp one at $f^* = 0.93$. These resonance frequencies can be observed in the results of the pressure sensor, too. The change of the speed of sound at different boundary conditions is within 0.3 %. The resonance frequency shift of acoustic dominant modes is well larger, thus, the influence of the speed of sound on the resonance frequencies is neglected in the further analysis. For increased pressure levels, the resonance frequencies diverge from each other. This behavior for coupled modes has been identified by Magara et al. (2008), too. They named the respective branches in-phase (decreasing resonance frequency for increasing pressure) and out-of-phase (increasing resonance frequency for increasing pressure) mode. The results of the pressure sensor in Figure 9 reveal a further resonance at $f^* = 0.97$ independent of the pressure level. This acoustic dominant mode is weakly or even not coupled to a structure dominant mode, because its resonance frequency is hardly dependent on the pressure level, but shows a linear dependency on the speed of sound. It is not considered in the further parts of the paper, which deal with the coupled modes only. The natural frequencies of the aforementioned three peaks are plotted over the density for a better overview in Figure 10.

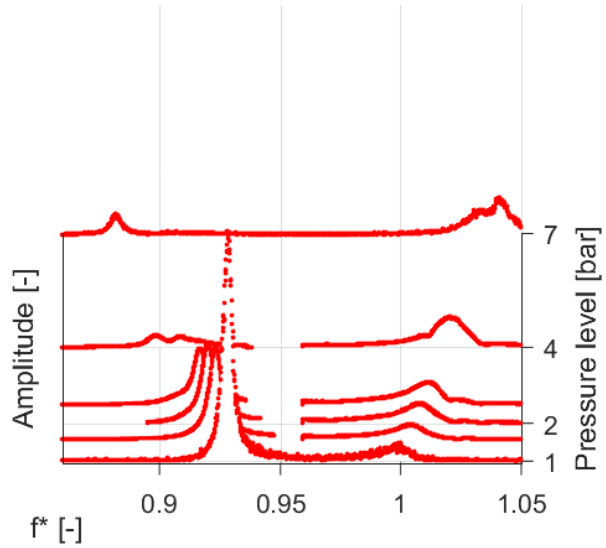

Figure 8: STFT results of frequency sweeps at different pressures (strain gage data).

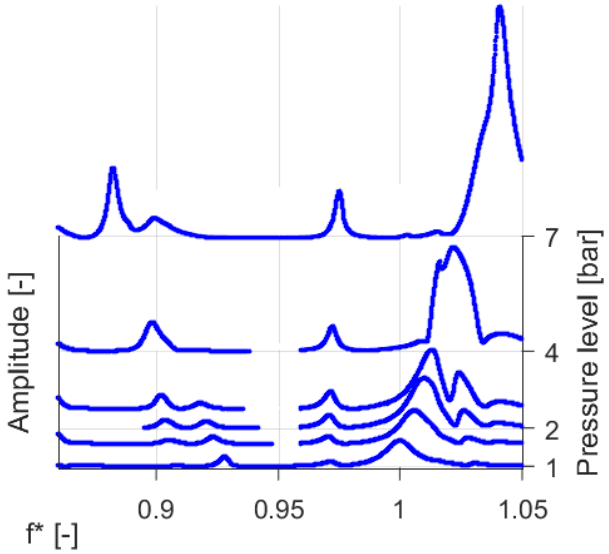

Figure 9: STFT results of frequency sweeps at different pressures (pressure sensor data).

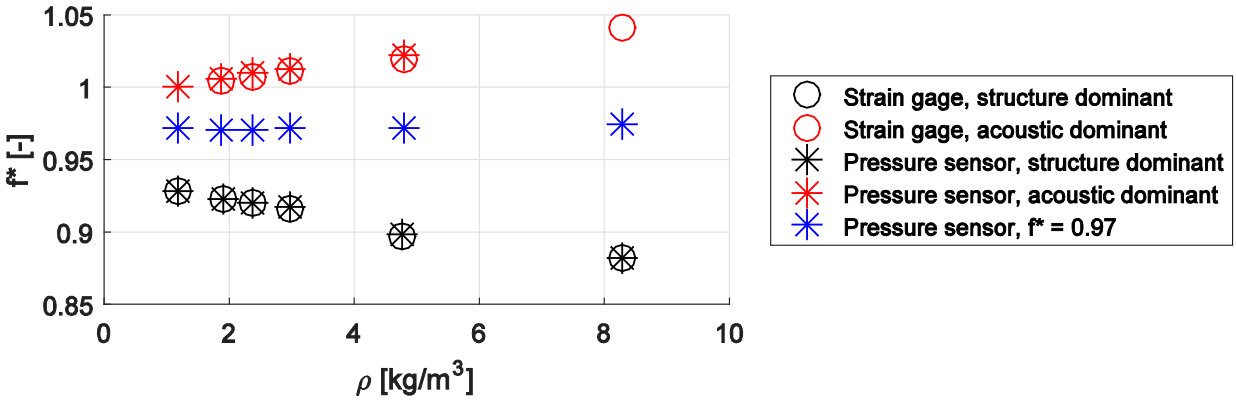

Figure 10: Overview of the resonance frequencies of the considered modes.

For further analysis a reliable determination of the actual mode shape at the respective resonance frequencies is important. Results of the rotatable sensor, for pressure pattern determination, are shown in Figure 11 and Figure 12 at a constant frequency of $f^* = 1$ and $f^* = 0.93$, respectively. The upper diagram indicates the pressure amplitude over the circumferential position in the test rig. In the lower diagram the circumferential pressure distributions for phase differences of approximately 1/12 π are plotted. The vertical dash-dotted line in each figure corresponds to the circumferential position of the exciting loudspeaker (LS).

The results in Figure 11 at an excitation frequency of $f^* = 1$ and a pressure of $p = 1$ bar show a clear modal shape with four nodes between 0° and 180° degree circumferential position. These nodes correspond to four nodal diameters in the complete cavity. A comparison of the phase difference between the pressure sensors P145 and P147 @ 50° shows an in-phase response signal. Thus, the excited mode is a pure nodal diameter mode with no nodal circles as expected based on the numerical coupled modal analysis. For the detection of an axial node the numerical modal analysis is used, too, which leads for the $m_{ac} = 4$, $n_{ac} = 0$, $l_{ac} = 1$ mode to a resonance frequency of $f^* = 0.994$, which is very close to the measured frequency of $f^* = 1$. Hence, the identification of the $m_{ac} = 4$, $n_{ac} = 0$, $l_{ac} = 1$ acoustic dominant mode at an excitation frequency of $f^* = 1$ can be highly probably concluded. The numerical modal analysis reveals an out-of-phase phase relation between the vibration of the structure and the pressure distribution.

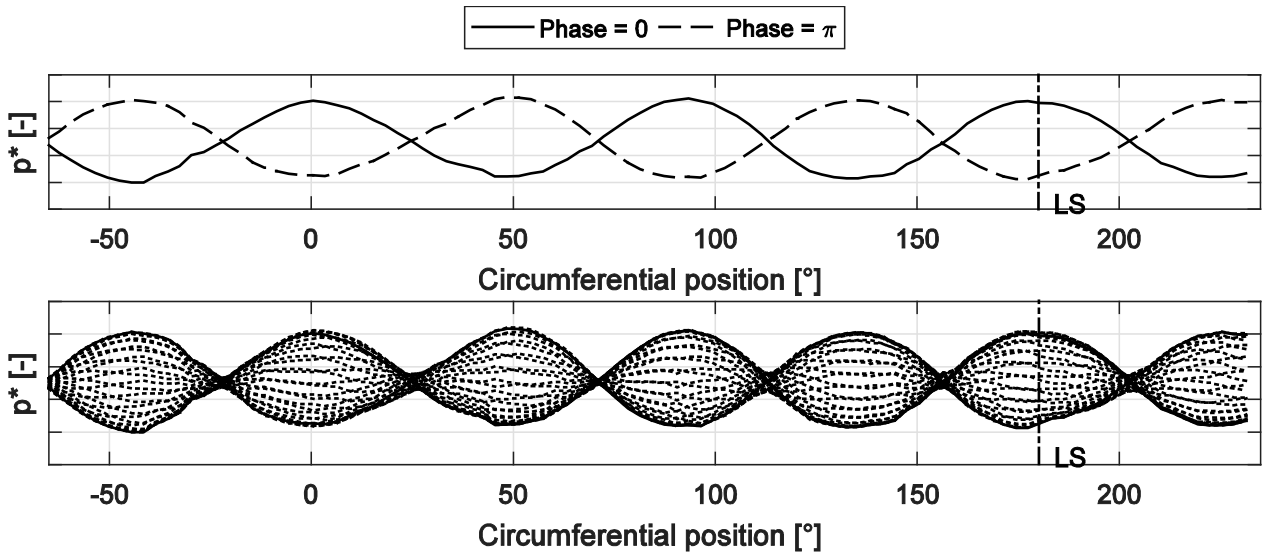

Figure 11: Results of the rotatable pressure sensor at *f = 1.**

The results of the rotatable pressure sensor at an excitation frequency of $f^* = 0.93$ and a pressure of $p = 1$ bar are drawn in Figure 12. In the upper diagram, indicating the pressure amplitude, four nodes can be identified between 0° and 180° degree circumferential position. Compared to the results of the acoustic dominant mode (Figure 11), the peak amplitudes are not equal to each other. Furthermore, the peak amplitude in the vicinity of the 0° circumferential position is shifted in its location about 8° degrees, which is a larger local shift than for the acoustic dominant mode (Figure 11). A reason could be an excitation frequency slightly differing from the exact resonance frequency of this mode. Due to the weak damping of this structure dominant mode it could lead to a misshaped pressure pattern. The phase relation between the pressure sensors P145 and P147 @ 50° shows their response signal in-phase, concluding the existence of a nodal circle to be very unlikely. Similar to the results with an excitation frequency of $f^* = 1$ the numerical modal analysis result is used as a further evidence for the identification of the mode. The calculated natural frequency of the structure dominant in-phase $m_{st} = 4$, $n_{st} = 0$ mode lies at $f^* = 0.936$. Thus, the excited modal shape at $f^* = 0.93$ can be very likely identified as the structure dominant in-phase $m_{st} = 4$, $n_{st} = 0$ mode with one axial node in the pressure pattern (l =1).

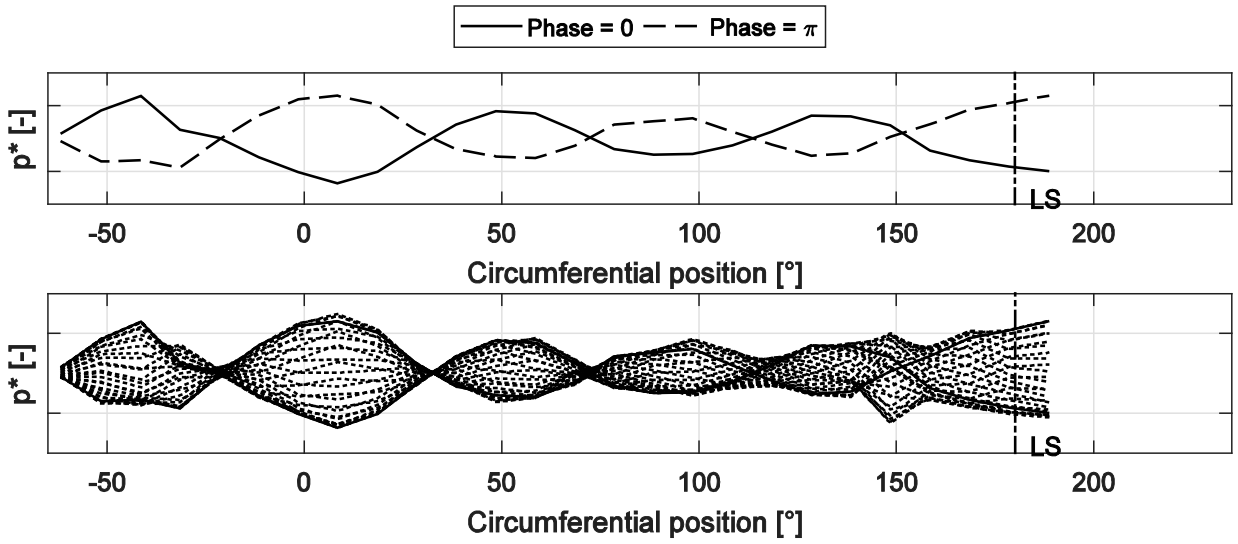

Figure 12: Results of the rotatable pressure sensor at *f = 0.93.**

Resonance Frequencies

In Figure 13 the dependency of the resonance frequencies of the acoustic dominant mode on the pressure level is presented. The experimental results are compared with the numerical modal analysis and the analytical results of Magara et al. (2008). In Figure 14 the relative deviations of the respectively determined resonance frequencies to the resonance frequency determined with the strain gage data is displayed. The following trends can be identified: The numerical modal analysis underestimates the resonance frequency compared to the experimental data at all densities, except for the 4.8 kg/m^3 case. The deviations of the numerical modal analysis and the analytical model remain similar until the densest case. The resonance frequency determined with the pressure sensor remains similar for all densities except the one at a density of 8.3 kg/m^3, where two acoustic modes are mixed and the resonance frequency cannot be determined clearly with the pressure sensor data. The resonance frequency gradients of the experimentally determined ones are flatter than the numerically and analytically determined ones. This could be an evidence for a weaker coupling of the acoustic dominant mode to the structure dominant mode in the real case than it is estimated numerically and analytically. An explanation could be found in the other branch, the structure dominant mode with four nodal diameters.

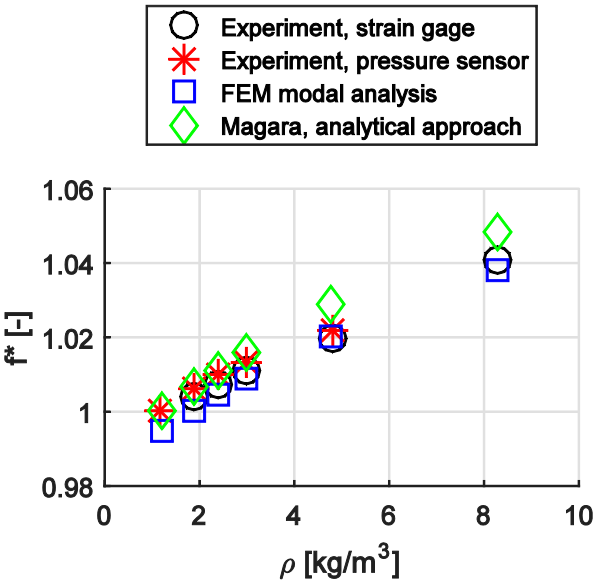

Figure 13: The resonance frequency of the acoustic dominant mode at different gas densities. Comparison of different results.

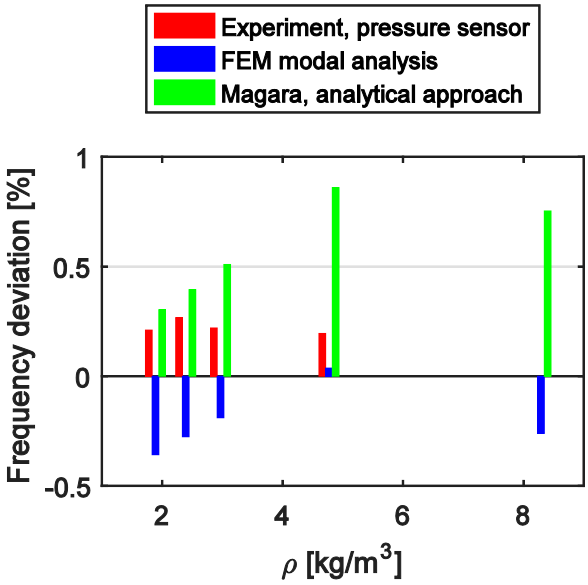

Figure 14: The relative resonance frequency deviation of the different results to the strain gage data. Acoustic dominant mode.

The results of the structure dominant mode at different gas densities are presented in Figure 15 and the relative deviations to the strain gage as a basis in Figure 16. The numerically determined resonance frequencies are higher compared to the experimentally determined resonance frequencies. Similar to the acoustic dominant mode the experimentally determined resonance frequencies have a flatter gradient than the numerically and analytically have until a density of 3 kg/m^3. As the density changes from 3 kg/m^3 to 4.8 kg/m^3 a discontinuity of the experimentally determined resonance frequencies is observed. It seems to have a stepwise change to a lower frequency. Probably another acoustic mode, which has not been identified, starting at f^* =0.91 and p = 1 bar (Figure 9) influences the identified acoustic dominant mode. A change of the eigenmodes could be likely, as Sigrist et al. (2006) have found out. However, a more thorough experimental investigation is necessary to clarify this finding. In the publication of Magara et al. (2008) a resonance frequency shift could be detected in the results, too, however, it is not mentioned by them.

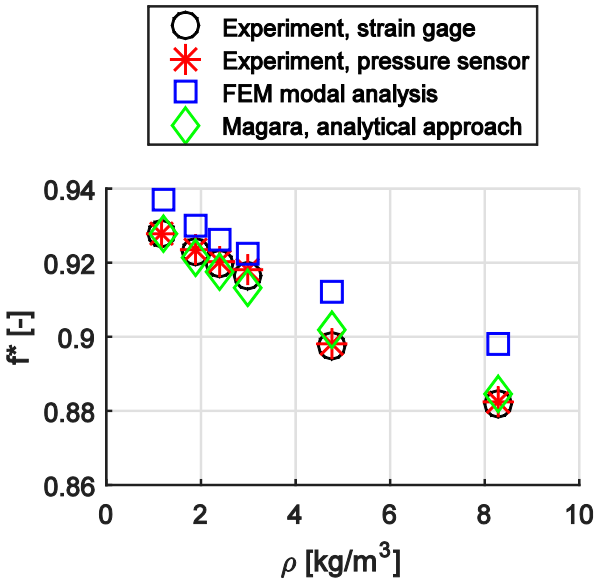

Figure 15: The resonance frequency of the structure dominant mode at different gas densities. Comparison of different results.

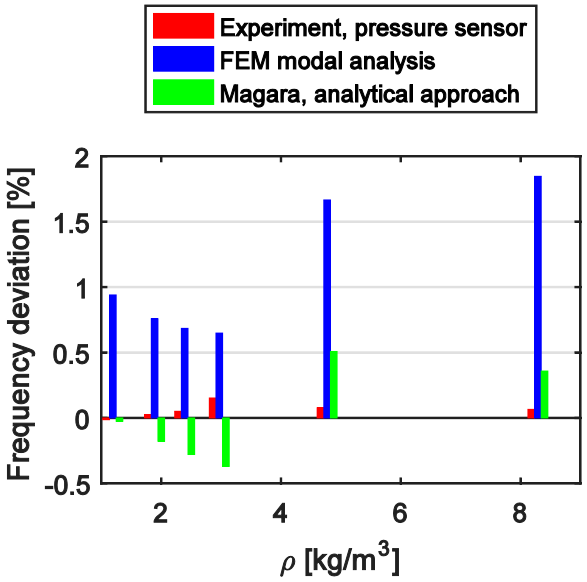

Figure 16: The relative resonance frequency deviation of the different results to the strain gage data. Structure dominant mode.

CONCLUSIONS

In this paper a rotor-stator cavity test rig for experimental investigations of acoustic fluid-structure interactions in side cavities of radial compressors is introduced. The instrumentation of the test rig and the evaluation methodology is presented. The fluid is excited at independent frequencies and the acoustic pressure patterns are detected with a rotatable pressure sensor.

First results of a pressure level variation and a stationary disk are presented. The structure and acoustic dominant m = 4, n = 0, l = 1 modes have been excited and identified. The application of a rotatable pressure sensor contributes essentially to the clear identification of them. The results of the coupled modes' resonance frequencies on the dependence of the surrounding gas pressure are in good accordance to previously published results of other researchers. Indications for a resonance frequency switch have been found for coupled modes, when their resonance frequencies converge to each other. This has been identified by researchers in other scopes of applications, too. Based on these preliminary investigations it can be concluded that crossing modes can have an influence on the resonance frequency of structure dominant modes, hence shifting them at specific gas properties in a different way than it is predicted by analytical and numerical tools.

ACKNOWLEDGMENTS

This project is funded by BMWi (Bundesministerium für Wirtschaft und Energie). The authors are grateful for the financial support under contract number 03ET2011E.

REFERENCES

Barabas, B., Clauss, S., Schuster, S., Benra, F.-K., Dohmen, H. J., Brillert, D., (2015). *Experimental and Numerical Determination of Pressure and Velocity Distribution Inside a Rotor-Stator Cavity at very High Circumferential Reynolds Numbers.* Proceedings of 11th European Turbomachinery Conference, 2015, Madrid, Spain

Cicon, D. E., Sofrin, T. G., Mathews, D. C., (1982), *Investigation of Continuously Traversing Microphone System for Mode Measurement.* NASA

Ehrich, F. F., (1969), *Acoustic Resonances and Multiple Pure Tone Noise in Turbomachinery Inlets.* In: ASME Journal of Engineering for Power, pp. 53-262

Ewins, D. J., (1995). *Modal Testing: Theory and Practice*. Research Studies Press

König, S., (2009), *Acoustic Eigenmodes in the Side Cavities of Centrifugal Compressors*. Proceedings of ASME Turbo Expo, Orlando, Florida, USA, GT2009-59650

Liang, Q. W., Rodríguez, C.G., Egusquiza, E., Escaler, X., Farhat, M., Avellan, F., (2007). *Numerical simulation of fluid added mass effect on a francis turbine runner*. In: Computers & Fluids, Vol. 36, pp. 1106-1118

Magara, Y., Narita, M., Yamaguchi, K., Takahashi, N., Kuwano, T., (2008). *Natural Frequencies of Centrifugal Compressor Impellers for High Density Gas Applications*. Proceedings of IMECE2008, Boston, Massachusetts, USA, IMECE2008-67278

Magara, Y., Yamaguchi, K., Miura, H., Takahashi, N., Narita, M., (2013). *Natural Frequency Shift in a Centrifugal Compressor Impeller for High-Density Gas Applications*. In: Journal of Turbomachinery, Vol. 135, pp. 011014-1 – 011014-8

Petry, N., (2011). *Experimentelle Untersuchung aeroakustischer und aeroelastischer Phänomene in Hochdruck-Radialverdichtern.* Ph.D. Dissertation, Universität Duisburg-Essen, Essen, Germany.

Rodriguez, C.G., Egusquiza, E., Escaler, X., Liang, Q. W., Avellan, F., (2006). *Experimental investigation of added mass effects on a Francis turbine runner in still water*. In: Journal of Fluids and Structures, Vol. 22, pp. 699-712

Sandberg, G., Göransson, P., (1988). *A Symmetric Finite Element Formulation for Acoustic Fluid-Structure Interaction Analysis*. In: Journal of Sound and Vibration, Vol. 123(3), pp. 507-515

Sigrist, J.-F., Broc, D., Lainé, C., (2006). *Dynamic analysis of a nuclear reactor with fluid-structure interaction Part I: Seismic loading, fluid added mass and added stiffness effects.* In: Nuclear Engineering and Design, Vol. 236, pp. 2431-2443

Tyler, J. M., Sofrin, T. G., (1961). *Axial Flow Compressor Noise Studies*. In: SAE Transactions, Vol. 70, pp. 309-332